ELSEVIER

Astroparticle Physics 14 (2001) 329–337

Astroparticle Physics

www.elsevier.nl/locate/astropart

Background discrimination capabilities of a heat and ionization germanium cryogenic detector

EDELWEISS Collaboration

P. Di Stefano [a,*], L. Bergé [b], B. Chambon [c], M. Chapellier [d], J. Chaumont [b], G. Chardin [a], P. Charvin [a,e], M. De Jésus [c], D. Drain [c], L. Dumoulin [b], P. Forget [d], P. Garoche [f], J. Gascon [c], C. Goldbach [g], D. L'Hôte [d], J. Mallet [a], J. Mangin [h], S. Marnieros [b], L. Miramonti [a], L. Mosca [a], X-F. Navick [a], G. Nollez [g], P. Pari [d], S. Pécourt [c], E. Simon [c], L. Stab [i], J-P. Torre [j], R. Tourbot [d], D. Yvon [a]

[a] *CEA, Centre d'Etudes Nucléaires de Saclay, DSM/DAPNIA, F-91191 Gif-sur-Yvette Cedex, France*
[b] *CSNSM, IN2P3-CNRS, Université Paris XI, bât. 108, F-91405 Orsay Cedex, France*
[c] *IPN Lyon and UCBL, IN2P3-CNRS, 43 Bd. du 11 novembre 1918, F-69622 Villeurbanne Cedex, France*
[d] *CEA, Centre d'Etudes Nucléaires de Saclay, DSM/DRECAM, F-91191 Gif-sur-Yvette Cedex, France*
[e] *Laboratoire Souterrain de Modane, CEA-CNRS, 90 rue Polset, F-73500 Modane, France*
[f] *Laboratoire de Physique des Solides, Université Paris XI, F-91405 Orsay Cedex, France*
[g] *Institut d'Astrophysique de Paris, INSU-CNRS, 98 bis Bd. Arago, F-75014 Paris, France*
[h] *LPUB, Université de Bourgogne, F-21078 Dijon, France*
[i] *Institut de Physique Nucléaire, Université Paris XI, F-91405 Orsay Cedex, France*
[j] *Service d'Aéronomie, BP 3, F-91371 Verrières le Buisson Cedex, France*

Received 21 March 2000

Abstract

The discrimination capabilities of a 70 g heat and ionization Ge bolometer are studied. This first prototype has been used by the EDELWEISS dark matter experiment, installed in the Laboratoire Souterrain de Modane, for direct detection of WIMPs. Gamma and neutron calibrations demonstrate that this type of detector is able to reject more than 99.6% of the background while retaining 95% of the signal, provided that the background events distribution is not biased towards the surface of the Ge crystal. However, the 1.17 kg day of data taken in a relatively important radioactive environment show an extra population slightly overlapping the signal. This background is likely due to interactions of low energy photons or electrons near the surface of the crystal, and is somewhat reduced by applying a higher charge-collecting inverse bias voltage (−6 V instead of −2 V) to the Ge diode. Despite this contamination, more than 98% of the background can be rejected while retaining 50% of the signal. This yields a conservative upper limit of 0.7 event $\mathrm{day}^{-1}\,\mathrm{kg}^{-1}\,\mathrm{keV}_{\mathrm{recoil}}^{-1}$ at 90% confidence level in the 15–45 keV recoil energy interval; the present sensitivity appears to be limited by the fast ambient neutrons. Upgrades in progress on the installation are summarized.

* Corresponding author. Address: Max-Planck-Institut für Physik, Föhringer Ring 6, D-80805 Munich, Germany.
E-mail address: distefano@mppmu.mpg.de (P. Di Stefano).

0927-6505/01/$ - see front matter
PII: S0927-6505(00)00127-4

PACS: 95.35.+d
Keywords: Dark matter; WIMP; Cryogenic detector

1. Introduction

The search for dark matter is one of the major challenges of contemporary physics. Despite extensive scans for massive compact halo objects (MACHOs) initiated by several groups [1–3], it appears at present that the local density of dark matter can hardly be composed of baryonic matter essentially. Indeed, recent results from these experiments indicate that a significant fraction of the MACHOs observed in the direction of the small magellanic cloud (SMC) are probably due to deflectors internal to the SMC, further reducing the possible amount of dark matter in the form of MACHOs in the halo itself [4].

The coincidence of the electroweak interaction scale (SUSY theory) with that required for weakly interacting massive particles (WIMPs) to contribute significantly to the solution of the dark matter problem is a further motivation for attacking the WIMPs direct detection challenge. In addition, these hypothetical particles represent an attractive solution to the problem of galaxy formation. Experimental efforts are underway to detect these particles, either indirectly, by searching for products of their annihilation in the core of the Sun or of the Earth, or directly, by detecting the interactions of the WIMPs themselves in ordinary matter, as first suggested in the mid 1980s [5,6].

The sensitivity of present experiments appears to be limited by the radioactive background rate of the detectors [7] and by the systematics of the rejection scheme using statistical identification methods based on pulse shape discrimination (PSD) techniques in NaI crystals [8–13]. The motivation for the development of cryogenic detectors is the possibility, when the heat measurement is coupled with a measurement of ionization [14–17] (or of scintillation [18]), to discriminate much more reliably the main source of radioactive background, producing electron recoils, from the nuclear recoils expected from WIMP interactions. Indeed, WIMPs scatter off nuclei, which ionize (or produce scintillation) less efficiently than electron recoils for a given energy deposit in the absorber.

In the following, we present the discrimination capabilities of this new generation of detectors in the Expérience pour Détecter les WIMPs en Site Souterrain (EDELWEISS) underground experiment and we show that a 70 g high-purity Ge crystal can already reach sensitivity levels typical of the best existing experiments despite its small mass and a relatively high radioactivity level in the detector environment. The present limitations of these detectors are then explored and the first attempts to counteract them are discussed.

2. The EDELWEISS experiment

The EDELWEISS cryogenic experiment operates in the Laboratoire Souterrain de Modane (LSM), an underground laboratory off the Fréjus highway tunnel beneath the French-Italian Alps. The 4600 mwe of rock reduce the muon flux to one part in two million of its surface value, i.e., to about 4.5 muons $m^{-2}\,day^{-1}$. The fast ambient neutron flux is measured to be 4×10^{-6} $cm^{-2}\,s^{-1}$ [19].

The cryogenic setup and shielding are presented in Ref. [20]. In particular, the dilution refrigerator has a cooling power of 100 μW at 100 mK, a useful volume for bolometer installation of about one liter and can reach temperatures as low as 10 mK. The optimized readout electronics are described in Ref. [21]. The results presented here concern a prototype germanium detector of only moderate radioactive cleanliness, without near Roman lead shielding, radon removal or ambient neutron moderator.

2.1. The cryogenic detector

The absorber of the detector consists in a 70 g germanium monocrystal of high purity ($n_D - n_A \cong$

5×10^9 cm^{-3}). The crystal shape is a disc 8 mm thick and 48 mm in diameter with bevelled edges.

Both charge and heat signals resulting from a particle interaction are measured by this detector. Charge collection is achieved by an electric field applied between two electrodes realized by boron implantation on one face of the monocrystal and by phosphorus implantation on the other. The applied bias voltages are of the order of a few volts. The p–i–n structure has been chosen to decrease, as much as possible, the injection of carriers in the detector volume and to allow large bias voltages. The doses of implanted ions are two orders of magnitude above the insulator–metal transition. The implantation energies have been chosen in order to reduce the thickness of the non-metallic implanted region and to ensure that the metallic layer reaches the detector surface. Recrystallization in the implanted region has been achieved by a fast thermal annealing and its quality checked by ellipsometry and by SIMS. [1] In addition, sheet resistances have been measured on this last detector to verify the metallic behavior at very low temperatures [22,23]. Several improvements of the detector design result from a study of the trap ionization and neutralization mechanisms in the bulk of the detector. The very low density of ionized traps we reached allows a noticeable improvement of the ionization channel time stability and energy resolution [23–28]. In order to minimize edge effects and to maximize charge collection, the thickness of the monocrystal has been reduced to 4 mm along its contour to increase the field strength, thereby reducing trapping and recombination.

The heat measurement is based on the variation, according to the Mott–Efrös–Schklovskii law, of the resistivity of a neutron transmutation doped (NTD) germanium. This thermal sensor is glued to one face of the detector. The size of this NTD is $2 \times 1 \times 0.8$ mm^3. The heat sink consists of three copper wires 50 μm in diameter and about 2 cm length. The operating temperature of the NTD sensor is about 20 mK for a mixing chamber temperature around 10 mK.

The whole detector lies on sapphire balls to ensure a good thermal decoupling from the detector holder made of low radioactivity copper and brass. A detailed description of the detector manufacturing and performances is given in Refs. [22–28].

2.2. Off-line data analysis

The small size of the heat and ionization signals (typically a temperature increase of $\approx 10^{-6}$ K, and of the order of a thousand electron–hole pairs) exposes them to various electronic noises, which may be fundamental or instrumental (Fig. 1). Therefore, analysis of the data has been performed off-line using various methods including the optimal filtering technique in Fourier space [29]. This involves a least square fit in frequency space between the actual event and a model event (obtained by averaging away the noise on several real events) while inversely weighting each frequency by the standard deviation of the noise at that frequency.

Neglecting pileup and assuming pulse shapes independent of pulse amplitude, each event s can be represented as the sum of a scaled and shifted model m and of a random noise n, $s(t) = Am(t - t_s) + n(t)$. Further assuming the noise to be gaussian in frequency space, we can construct a χ^2

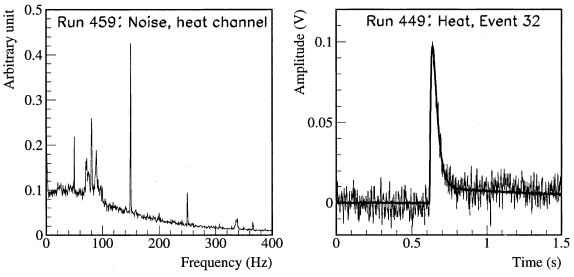

Fig. 1. Left: a noise spectrum of the heat channel. Overall shape is that of thermodynamical noise level of the NTD, squashed by low-pass filter. Two types of peaks are visible: narrow electromagnetic ones essentially due to the odd harmonics of the electrical supply, and wider ones due to microphonics. Right: result of optimal filter fit on a heat event (≈60 keV).

[1] Second Ionisation Mass Spectroscopy. These electrode characterizations have been done with a previous detector by J.-P. Ponpon of the PHASE Laboratory (Strasbourg, France).

as the weighted difference between signal and scaled and shifted model [29]:

$$\chi^2 = \sum_{\omega} \frac{|N(\omega)|^2}{\sigma_\omega^2} = \sum_{\omega} \frac{|S(\omega) - A\mathrm{e}^{-\mathrm{i}\omega t_s} M(\omega)|^2}{\sigma_\omega^2},$$

where σ_ω is the standard deviation of the noise at frequency $\omega/2\pi$ and capital letters represent the Fourier transform of their lowercase counterparts. Minimization with respect to A and t_s yields an estimate of these two parameters. Parseval's identity allows us to simply maximize over time shifts the scalar product $A = \sum_t f(t - t_s)s(t)$, where the function f can be calculated from its Fourier transform once for all events [30]

$$F(\omega) = \mathrm{e}^{-\mathrm{i}\omega t_s} \frac{M(\omega)}{\sigma_\omega^2} \Big/ \sum_{\omega} \frac{|M(\omega)|^2}{\sigma_\omega^2}.$$

Calculating the χ^2 to judge the quality of the fit is however more tractable in frequency space, and this remains computationally feasible thanks to fast Fourier transforms.

With respect to time fit techniques, this method selectively filters out noisy frequencies and thus is advantageous in the many cases of non-white noise spectra (Fig. 1). Like straightforward time fit techniques however, it is ill-suited to data presenting pileups, though given current masses of bolometers this is not yet a problem when looking for WIMPs.

3. In situ detector calibrations

3.1. Energy normalization and recoil energy determination

The heat signal results from the sum of the heat deposited by the incident particle and of the heat generated by the charge carriers during their drift (the so-called Luke-Neganov effect [31]). This last term is given by the product of the bias voltage by the collected charge. Thus as bias voltage increases, the fraction of the heat signal directly correlated to the ionization signal increases, hampering separation of the electron recoils from the nuclear recoils. In practice, although bias voltages up to -12 V have been used, most of the data have been accumulated under bias voltages of -2 and -6 V. There is in fact an additional electric field to that applied; it is caused by the 0.7 eV gap in Ge which creates a -0.7 V reverse field in the p–i–n diode. However, only the applied field ultimately counts for the Luke-Neganov effect: the energy equal to the additional field times the collected charge is indeed released when the charges are collected, but merely compensates the energy used to create the pairs in the first place [32].

Moreover, it is a standard procedure to normalize heat (phonon) energies (keV heat) to equivalent electron energies (keV e.e). Volume electron recoils (with almost complete charge collection) are used to calibrate the charge and phonon channels. For such a volume electron recoil of a given energy (e.g. 122 keV for a ^{57}Co calibration), both charge and phonon amplitudes (E_{ch} and E_{ph}, respectively) are normalized to the deposited energy. In order to reconstruct this energy deposited in the detector, or recoil energy E_{rec}, from these quantities, the following formula [31,33] is applied:

$$E_{\mathrm{rec}} = E_{\mathrm{ph}}\left(1 + \frac{eV}{\epsilon_\gamma}\right) - E_{\mathrm{ch}}\frac{eV}{\epsilon_\gamma},$$

where V is the bias voltage for charge collection (V), e, the elementary charge and ϵ_γ, the average energy per electron–hole pair (eV) for an electron recoil. The recoil energy resolution becomes thus bias-dependent, as shown in Fig. 6. In the absence of Luke-Neganov effect ($V = 0$) $E_{\mathrm{rec}} = E_{\mathrm{ph}}$; for a photon interaction where all the charge is collected (volume electron recoil), $E_{\mathrm{rec}} = E_{\mathrm{ph}} = E_{\mathrm{ch}}$.

It is shown in Refs. [33,34], how the ϵ_γ parameter can be measured using, in X- and γ-ray line calibrations, the small fractions of events which exhibits an incomplete charge collection. The measured value is close to the standard value $\epsilon_\gamma \cong 3$ eV for the 77 K germanium diode detectors [35].

3.2. Electron recoil thresholds and resolutions

Electron recoil energy resolutions and thresholds have been studied using a ^{57}Co source which provides essentially photoelectric interactions

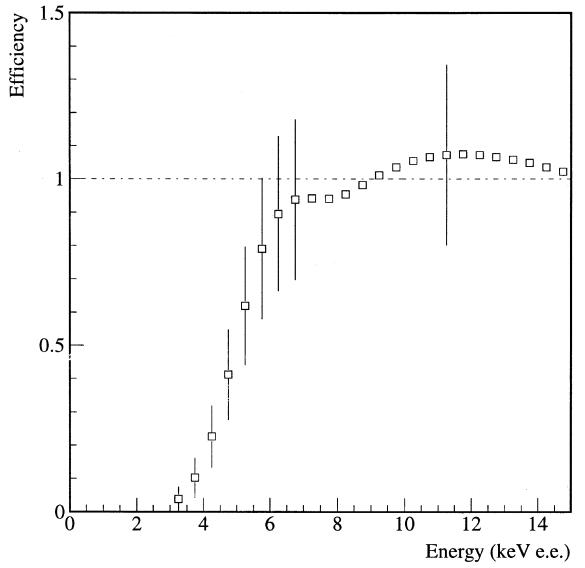

Fig. 2. The threshold efficiency of the ionization channel, determined by comparing the data of ^{60}Co calibrations with a Monte-Carlo simulation.

from its main peak at 122 keV. The ionization signal being roughly 1000 times faster than the heat signal, the former has usually been used as trigger for the acquisitions with an effective threshold at 4 keV equivalent electron (e.e.) on the charge channel. Threshold efficiency has been studied by comparing a ^{60}Co calibration with a Monte-Carlo simulation. It is found to rise rapidly to 100% by 6 keV [36] (Fig. 2).

The heat and ionization channels exhibit energy FWHM resolution of $\approx$1 and $\approx$1.2 keV e.e. at 122 keV. According to the $E_{\rm rec}$ expression of Section 3.1, the corresponding resolutions on the recoil energy are $\approx$1.8 keV at -2 V and $\approx$3.8 keV at -6 V.

3.3. Signal and background calibrations

The detector has been calibrated with both neutron and gamma sources in order to check its power of separation between nuclear recoil (“signal”) and electron recoil (background) events. High energy photons provide Compton interactions throughout the crystal rather than biased towards its surface.

A ^{252}Cf neutron source, of about 2.5μCi activity, has been used for this calibration at two different values of the reverse bias voltage (-2 and -6 V). The branching ratio for neutron emission in the decay of the ^{252}Cf isotope is about 12% and the average kinetic energy of the emitted neutrons is around 2 MeV. The ^{252}Cf isotope is also a gamma source with a branching ratio of about 60%, and about 80% of these gammas have energy less than 1 MeV. So, in principle, this source alone is sufficient to obtain simultaneously both neutron and gamma calibrations. In order to improve the statistics without too long an exposure of the detector to the neutron source and the associated risk of neutron activation, we use also a ^{60}Co source to mimick the background noise of electron recoils. Results are presented in Fig. 3 for both polarization voltages, showing a remarkably good separation between gamma and neutron recoil events down to low energy. While most electron recoil events appear well behaved, and neatly line up along the main diagonal in the heat-ionization plane, approximately 5% suffer from incomplete charge collection.

The recoil energy $E_{\rm rec}$ is derived according to Section 3.1. Merging the data obtained at the two bias voltages yields the quenching factor $(E_{\rm ch}/E_{\rm rec})$ versus $E_{\rm rec}$ in Fig. 4. The curve 4 keV/$E_{\rm rec}$, which represents the threshold (at 4 keV e.e.), is also given. A “neutron line” (the quenching factor for nuclear recoils) can be parameterized using the measured spreads and mean values of the charge over recoil ratio, calculated in discrete recoil energy intervals above 20 keV (under 20 keV, a

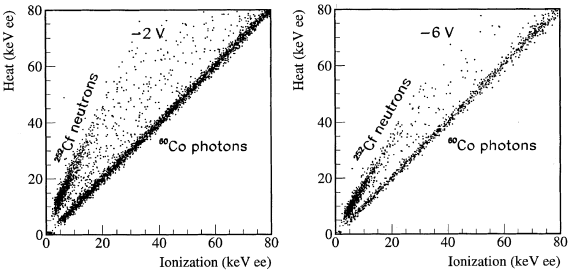

Fig. 3. Heat-ionization planes of ^{60}Co and ^{252}Cf calibrations at two bias voltages. Over the 0–80 keV e.e. energy interval, 5% of the events from ^{60}Co are ionization deficient at -2 V and 3% at -6 V.

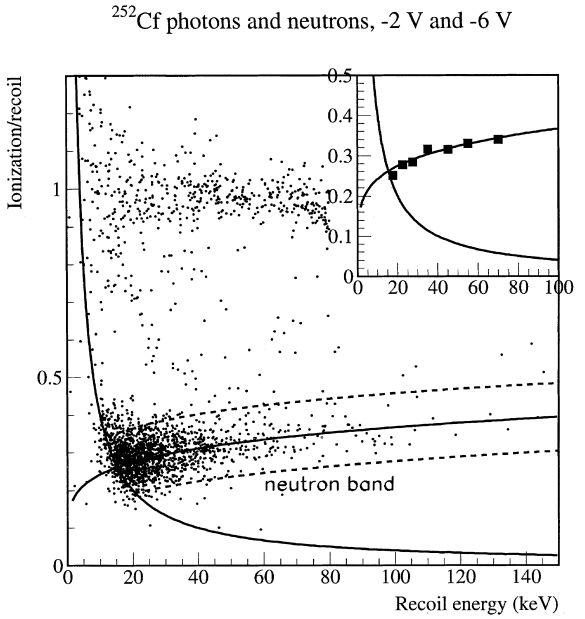

Fig. 4. The quenching factor, or ionization over recoil energy ratio, as a function of the recoil energy. To improve the statistics, the ^{252}Cf data collected at -2 and -6 V are merged. A neutron zone which contains 95% of the nuclear recoils is represented. The inset shows the agreement with the CDMS results [14] ((■) the extension of which is the order of the error bar).

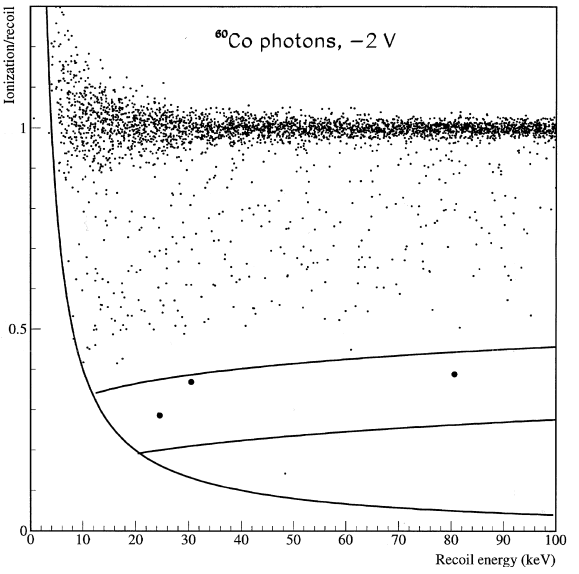

Fig. 5. Separation of signal from background based upon ^{60}Co photon calibration at -2 V bias voltage. 3229 events are found over the 15–100 keV recoil energy interval but only 3 remain in the 95% acceptance nuclear recoil band.

threshold bias is clearly visible). We obtain $E_{ch}/E_{rec} = (0.16 \pm 0.07)\ E_{rec}^{0.18\pm0.1}$, a result in agreement (within error limits) with those of the Heidelberg–Moscow collaboration [37], parameterized in [7] by $E_{ch} = 0.14E_{rec}^{1.19}$, and in turn in agreement with the Lindhard theory [38] and most of the previous experiments (see Ref. [37] and references therein). The comparison with the results of the CDMS experiment [14], shown in Fig. 4 inset, shows a very good agreement.

A neutron zone of known acceptance can be constructed by adjusting a power law of the recoil energy to the points at $+n\sigma$, $-m\sigma$ above and below the mean charge over recoil ratio. For a given background, the choice of the n and m values is a matter of optimizing the signal-to-noise ratio. In Fig. 4, the 95% acceptance neutron zone ($\pm 2\sigma$) is shown as an example. This neutron calibration induces a slight bias in the determination of the quenching factor: the non-negligible number of multiple diffusions in the crystal leads to a merging of the quenching factor values at different energies. The width of the nuclear recoil band is overestimated accordingly for WIMPs for which it should by single interactions only.

We now turn our attention to the separation capabilities of the detector based on the two types of calibration just discussed. In Fig. 5, we apply the neutron zone method to the data of the ^{60}Co calibration taken at -2 V. In the 15–100 keV recoil energy interval, three events (out of 3229) are found within the 95%-acceptance nuclear recoil band: $(99.90 \pm 0.05)\%$ of photon background is rejected. At -6 V, we find a rejection of $(99.6 \pm 0.2)\%$. These results are very promising; however, it must be kept in mind that they have been obtained from calibrations and that operational values may differ as we will see later.

4. A realistic case of data taking

Following the benchmarks just discussed, 0.65 kg day and 1.17 kg day of data were taken at the bias voltages of -2 and -6 V, respectively. Both

spectra show a rate of roughly ≈35–40 event $\mathrm{kg^{-1}\,day^{-1}\,keV_{recoil}^{-1}}$ in the 15–45 keV recoil energy interval, below the 46.5 keV peak due to ^{210}Pb contamination. The recoil energy versus ionization plots of the data (Fig. 6) show a large number of off-axis events. This population, interpreted as incomplete charge collection of electron surface events, is discussed in Ref. [34] together with another population which appears at recoil energies of the order of 80–100 keV and is attributed to surface nuclear recoils.

Given the large number of events with incomplete charge collection, we only retain the $(0\sigma, -2\sigma)$ neutron zones as discussed in Section 3 (Fig. 7). This improves the signal-to-noise ratio and halves the acceptance to 0.475. The samples recorded respectively at −2 and −6 V bias contain six events (respectively seven events) in the 15–45 keV recoil range. We assume they are nuclear recoils, and use them to derive a conservative upper limits on a signal. For the respective exposures and acceptance, they yield upper limits at the 90% confidence level of 1.1 event $\mathrm{kg^{-1}\,day^{-1}\,keV_{recoil}^{-1}}$ at −2 V, and 0.7 event $\mathrm{kg^{-1}\,day^{-1}\,keV_{recoil}^{-1}}$ at −6 V. It will appear below that a large fraction of the events observed in the nuclear recoil band can probably be attributed to neutron interactions inside the detector. One can thus only set a lower limit of 98% for the rejection factor of the electron recoil background.

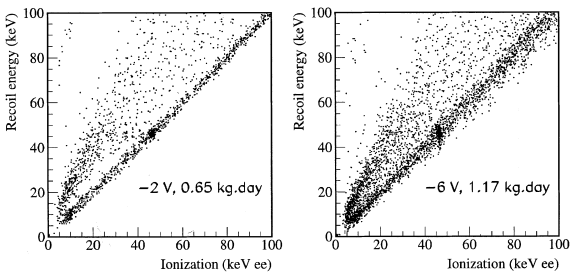

Fig. 6. Data at −2 and −6 V. Deriving recoil energies from the heat signal by the subtraction of charge times bias voltage causes the recoil energy resolution to become bias dependant, as can be seen on the 46.5 keV peak of ^{210}Pb.

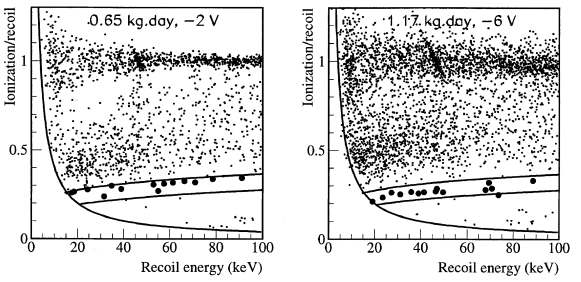

Fig. 7. Neutron zones and data at −2 and −6 V. We only retain the $(0\sigma, -2\sigma)$ neutron zones (47.5% acceptance) where 14 and 15 events (●●●) subsist, respectively over the 15–100 keV recoil energy range.

When we compare the mean ionization over recoil energy ratio of the off-axis events (electron surface events) at both bias voltages (0.46 ± 0.01 at −2 V and 0.539 ± 0.006 at −6 V), we find that the higher bias voltage brings the off-axis events significantly closer to the well-collected events.

We have also run the detector using a heat trigger. Because the ionization signal is roughly 1000 times faster than the heat signal, it is not always possible to correlate the pulse with the charge pulse. Nonetheless, this trigger mode has brought to light a distinct second type of thermal event, one with a rise time dominated by electronics and practically never correlated with an ionization event. For these two reasons, we attribute these events to interactions in the heat sensor itself. The energy spectrum of these events is compatible with a small amount of tritium activity in the NTD thermometer.

The events surviving in the neutron zone are not sufficiently separated from the population of electron surface events to be attributed with certainty to nuclear recoil events, induced in the Ge detector by ambient neutrons (the observed rate being much higher than what would be expected from WIMPs [7–10]). The flux and energy spectrum of the fast ambient neutrons originating for the most part from internal radioactivity in the surrounding rock have been measured in the LSM by our collaboration using conventional scintillation detectors. The flux was found to be $4.0 \pm 0.1\ 10^{-6}$ $\mathrm{cm^{-2}\,s^{-1}}$ (statistical error only) [19]. A Monte-Carlo simulation was then performed to predict the expected number of neutron-induced nuclear recoils in our 70 g Ge detector. It uses the GEANT Monte-Carlo simulation [39] in conjunction with a package specially developed [40] to handle low

Table 1
Measured number of events and simulated number of ambient neutron events in the nuclear recoil band (47.5% acceptance) over 15–100 keV recoil energy[a]

Bias voltage (V)	Exposure (kg day)	Measured recoil number	Simulated neutron number
−2	0.65	14 ± 4	7 ± 2
−6	1.17	15 ± 4	12 ± 3

[a] The error bars on the simulated neutron numbers result from the experimental error on the measured neutron flux.

energy neutrons (from a few eV to a few MeV). The expected and measured number of recoils in the nuclear recoil band (47.5% acceptance) over the recoil energy interval 15–100 keV are given in Table 1.

By inspection of Table 1, it appears that at the −6 V polarization a large fraction, and possibly all the events observed in the nuclear recoil region can be attributed to neutron interaction inside the detector. At −2 V, however, the separation between nuclear recoils and electron surface events is, as already noted, slightly less favorable, and accordingly the simulation indicates a pollution of the nuclear recoil band by surface events.

5. Conclusion and outlook

Our prototype heat and ionization bolometer provides an excellent separation of the calibrated background and signal down to an energy of 4 keV e.e. However, data taken during background runs contain an important population of off-axis events (electron surface events) essentially not seen during the calibrations. Despite this, the rejection capabilities of the detector remain satisfactory, still reducing the number of electron recoil events by nearly two orders of magnitude. Sensitivity limits on WIMPs [16,17] obtained with this prototype are only a factor of 10 higher than the best existing limits obtained with longer-established techniques [7–10] despite the small mass (70 g) of our detector and the relatively high radioactivity level in the detector environment. Moreover, the present sensitivity of the experiment appears to be limited, principally for the runs with a −6 V bias voltage, not by the gamma background or by parasitic electron surface events, but by the ambient neutrons in the underground laboratory. Given the systematic uncertainties in the Monte-Carlo neutron simulations, a background subtraction is not attempted, but, clearly, shielding against neutrons is required.

A new generation of detectors is being tested in the LSM with new implantation schemes for the electrodes and a rigorous selection procedure of the crystal holder material [41]. Several improvements have been undertaken in the detector environment: nitrogen flushing for radon removal, improved passive protection against gamma radioactivity (including close Roman lead shielding) and 30 cm removable paraffin shielding against neutrons. In an initial test run, two 70 g prototypes show background levels before rejection of ≈ 2 event $\mathrm{keV}^{-1}\,\mathrm{kg}^{-1}\,\mathrm{day}^{-1}$ below 50 keV, a factor of 10 improvement over previous data, with a comparable progression for electron surface events. The number of events remaining in the neutron zone is now extremely limited and could be due to residual neutron interactions inside the present shielding. Assuming a good performance of the neutron shielding and that the energy resolution and background rejection are the same as those reported here, a few months of data taking with these detector should allow a test of the entire parameter region claimed by the DAMA experiment [8–10], and the entrance into the relevant supersymmetry parameter space.

Acknowledgements

The support of the technical staff of the Laboratorie Souterrain de Modane and of the participating laboratories is gratefully acknowledged. We thank J.P. Passerieux, A. Le Coguie and B. Cahan for the quality of their contribution to the drawing and realization of electronic components.

This work has been partially funded by the EEC-Network program under contract ERB-FMRXCT980167.

References

[1] C. Alcock, et al. (MACHO Collaboration), Nature 365 (1993) 621.
[2] E. Aubourg, et al. (EROS Collaboration), Nature 365 (1993) 623.
[3] B. Paczynski, et al., Bull. Am. Astron. Soc. 187 (1995) 1407.
[4] C. Alcock, et al. (EROS and MACHO Collaborations), Ap. J. 499 (1998) L9.
[5] A. Drukier, L. Stodolsky, Phys. Rev. D 30 (1984) 2295.
[6] M.W. Goodman, E. Witten, Phys. Rev. D 31 (1985) 3059.
[7] L. Baudis, et al., Phys. Rev. D 59 (1999) 022001.
[8] R. Bernabei, et al., Phys. Lett. B 389 (1996) 757.
[9] R. Bernabei, et al., Phys. Lett. B 424 (1998) 195.
[10] R. Bernabei, et al., Phys. Lett. B 450 (1999) 448.
[11] P.F. Smith, et al., Phys. Lett. B 379 (1996) 299.
[12] P.F. Smith, et al., Phys. Rep. 307 (1998) 275.
[13] G. Gerbier, et al., Astropart. Phys. 11 (1999) 287.
[14] T. Shutt, et al., Phys. Rev. Lett. 69 (1992) 3425.
[15] R.W. Schnee, et al., Phys. Rep. 307 (1998) 283.
[16] D. Drain, et al., Phys. Rep. 307 (1998) 297.
[17] L. Bergé, et al., Nucl. Phys. B 70 (1999) 69.
[18] P. Meunier, et al., Appl. Phys. Lett. 75 (1999) 1335.
[19] V. Chazal, et al., Astropart. Phys. 9 (1998) 163.
[20] A. de Bellefon, et al., Astropart. Phys. 6 (1996) 35.
[21] D. Yvon, et al., Nucl. Instr. Meth. Phys. Res. A 368 (1996) 778.
[22] D. L'Hote, et al., Nucl. Instr. Meth. Phys. Rev A 370 (1996) 193.
[23] X.-F. Navick, Thèse Doctorat, No 97/PA07/7146, Université Paris VII, 1997, unpublished.
[24] X.-F. Navick, et al., Nucl. Instr. Meth. Phys. Res. A 442 (2000) 267.
[25] X.-F. Navick, et al., Nucl. Instr. Meth. Phys. Res. A 370 (1996) 213.
[26] X.-F. Navick, et al., in: S. Cooper (Ed.), Proceedings of the Seventh International Workshop on Low Temperature Detectors, Munich, Germany, 1997, p. 244.
[27] D. L'Hôte, et al., Czechoslovak J. Phys. 46-S5 (1996) 2903.
[28] D. L'Hôte, et al., J. Appl. Phys. 87 (2000) 1507.
[29] S.H. Moseley, J.C. Mather, D. Mc Cammon, J. Appl. Phys. 56 (1984) 1257.
[30] A.E. Szymkowiak, R.L. Kelley, S.H. Moseley, C.K. Stahle, J. Low Temp. Phys. 93 (1993) 281.
[31] P.N. Luke, J. Appl. Phys. 64 (1988) 6858.
[32] T. Shutt, et al., Phys. Rev. Lett. 69 (1992) 3531.
[33] P. Di Stefano, Thèse de Doctorat, Université Paris XI Orsay, 1998, unpublished.
[34] A. Benoit, et al., Phys. Lett. B, 479 (2000) 8.
[35] G.E. Knoll, Radiation Detection and Measurement, Wiley, New York, 1989.
[36] L. Miramonti, Thèse de Doctorat, Université Paris XI Orsay, 1999, unpublished.
[37] L. Baudis, et al., Nucl. Instr. Meth. Phys. Res. A 418 (1998) 348.
[38] J. Lindhard, V. Nielsen, M. Scharff, P.V. Thomsen, Mat. Fyz. Medd. Dan. Vid. Selsk. 33 (1963) 1.
[39] GEANT Detector Description and Simulation Tool, CERN Program Library, W5103, CERN, 1993.
[40] H. de Kerret, B. Lefièvre, Report, Collège de France, LPC 88 01, 1988, unpublished.
[41] X.-F. Navick, et al., Nucl. Instr. Meth. Phys. Res. A 444 (2000) 361.